

Temporary pause in the growth of atmospheric ethane and propane in 2015-2018

Hélène Angot^{1,2}, Connor Davel¹, Christine Wiedinmyer³, Gabrielle Pétron^{3,4}, Jashan Chopra¹, Jacques Hueber^{1,5}, Brendan Blanchard¹, Ilann Bourgeois^{3,6}, Isaac Vimont³, Stephen A. Montzka⁴, Ben R. Miller^{3,4}, James W. Elkins⁴, Detlev Helmig^{1,5}.

¹Institute of Arctic and Alpine Research, University of Colorado Boulder, Boulder, CO, USA.

²~~Extreme Environments Research Laboratory~~, École Polytechnique Fédérale de Lausanne (EPFL) Valais Wallis, Sion, Switzerland.

³Cooperative Institute for Research in Environmental Sciences, University of Colorado Boulder, Boulder, CO, USA.

⁴NOAA, Global Monitoring Laboratory (GML), Earth System Research Laboratories, Boulder, CO, USA.

⁵Boulder A.I.R. LLC, Boulder, CO, USA.

⁶NOAA, Chemical Sciences Laboratory (CSL), Earth System Research Laboratories, Boulder, CO, USA.

Correspondence to: Hélène Angot (helene.angot@epfl.ch)

Abstract.

Atmospheric non-methane hydrocarbons (NMHCs) play an important role in the formation of secondary organic aerosols and ozone. After a multidecade global decline in atmospheric mole fractions of ethane and propane – the most abundant atmospheric NMHCs – previous work has shown a reversal of this trend with increasing atmospheric abundances from 2009 to 2015 in the Northern Hemisphere. These concentration increases were attributed to the unprecedented growth in oil and natural gas (O&NG) production in North America. Here, we supplement this trend analysis building on the long-term (2008-2010; 2012-2020) high-resolution (~ 3-hour) record of ambient air C₂-C₇ NMHCs from in-situ measurements at the Greenland Environmental Observatory at Summit station (GEOSummit, 72.58°N, 38.48°W, 3210 m above sea level). We confirm previous findings that the ethane mole fraction significantly increased by +69.0 [+47.4, +73.2; 95 % confidence interval] ppt per year from January 2010 to December 2014. Subsequent measurements, however, reveal a significant decrease by -58.4 [-64.1, -48.9] ppt per year from January 2015 to December 2018. A similar reversal is found for propane. The upturn observed after 2019 suggests, however, that the pause in the growth of atmospheric ethane and propane might only have been temporary. Discrete samples collected at other northern-hemisphere baseline sites under the umbrella of the NOAA cooperative global air sampling network show a similar

Formatted: French (Switzerland)

Deleted: School of Architecture, Civil and Environmental Engineering...

Deleted: The analysis of 2012-2019 air mass back-trajectories shows that this pause in mole fraction increases can neither be attributed to changes in atmospheric transport nor to changes in regional emissions.

decrease in 2015-2018 and suggest a hemispheric pattern. Here, we further discuss the potential contribution of biomass burning and O&NG emissions, the main sources of ethane and propane, and we conclude that O&NG activities likely played a role in these recent changes. This study highlights the crucial need for better constrained emission inventories.

Deleted: , however,

1. Introduction

Non-methane hydrocarbons (NMHCs) are emitted to the atmosphere by a variety of biogenic and anthropogenic sources. Their atmospheric oxidation contributes to the production of surface ozone and aerosols, with impacts on air quality and climate forcing (Houweling et al., 1998). The abundance of the most abundant atmospheric NMHCs (ethane, propane, i-butane, n-butane, i-pentane, n-pentane) increased steadily after 1950 until reduced emissions from oil and natural gas (O&NG) production and emission regulations from diverse sources (*e.g.*, automobiles and industrial processes) began to be implemented in the 1970s (Helmig et al., 2014). Emission reductions led to a gradual decline (3-12 % per year) of NMHCs at urban and semi-rural sites in the last five decades (*e.g.*, von Schneidemesser et al., 2010; Warneke et al., 2012). Accounting for an approximate atmospheric lifetime (at $\text{OH} = 6.5 \times 10^5 \text{ molecules/cm}^3$) ranging from 4.5 days for pentanes to 2 months for ethane, these emission reductions are also reflected in observations of background air composition, as seen in Northern Hemisphere firm air records (Aydin et al., 2011; Worton et al., 2012; Helmig et al., 2014): light alkanes increased steadily post 1950, peaking ~50 % above 1950 levels around 1970-1985, and then steadily declined until 2010 to levels that were close to 1950 levels. After some 40 years of steadily declining atmospheric ethane and propane mixing ratios, Helmig et al. (2016) reported a reversal in this behavior: the analysis of weekly discrete air samples has shown that between mid-2009 and mid-2014, ethane abundance at surface sites in the Northern Hemisphere increased at a rate of 2.9-4.7 % per year. These observations and conclusions were further substantiated by solar Fourier transform infrared (FTIR) ethane column retrievals showing similar increases in the mid to upper tropospheric ethane column (Franco et al., 2015, 2016; Hausmann et al., 2016). The largest increase rates for ethane and propane mixing ratios were found at sites located in the Eastern United States (U.S.) and in the Northern Atlantic Region, indicating larger emissions from the central to eastern parts of the U.S., with the likely sources being increased emissions from shale O&NG extraction operations.

68 Interestingly, there is a strong latitudinal gradient of absolute NMHC dry air mole fractions – with
69 highest abundances in the Arctic where atmospheric removal rates are low during the polar winter
70 (Helmig et al., 2016, 2009; Rudolph, 1995). Despite the sensitivity of the Arctic to pollution
71 transport from lower latitudes, climate change, and already recognized and further anticipated
72 feedbacks on the global climate, long-term in-situ atmospheric composition observations within
73 the Arctic are sparse. A large part of our current knowledge of polar atmospheric chemistry stems
74 from research aircraft missions and campaign-type observations (e.g., Hartery et al., 2018; Jacob
75 et al., 2010; Law et al., 2014). However, long-term continuous measurements or regularly repeated
76 observations with consistent methodology and instrumentation are indispensable for establishing
77 a baseline record of environmental conditions at clean remote sites and for observing their changes
78 over time. Such data also serve as a legacy for future research that will rely on comparison with
79 archived observations of environmental conditions.

80 In that context, the National Oceanic and Atmospheric Administration (NOAA) Global
81 Monitoring Laboratory (GML) initiated a cooperative air-sampling network at Niwot Ridge,
82 Colorado, in 1967 (hereafter referred to as the NOAA/GML Carbon Cycle Greenhouse Gases
83 (CCGG) network (<https://www.esrl.noaa.gov/gmd/ccgg/>)). This network is nowadays an
84 international effort and discrete air samples are collected approximately weekly from a globally
85 distributed network of sites, including four Arctic sites: Utqiagvik (formerly known as Barrow,
86 Alaska, USA), Alert (Nunavut, Canada), Summit (Greenland), and Ny-Ålesund (Svalbard,
87 Norway). These samples are analyzed for CO₂, CH₄, CO, H₂, N₂O, and SF₆ at GML (e.g., Geller
88 et al., 1997; Komhyr et al., 1985; Steele, 1991), and at the University of Colorado Institute for
89 Arctic and Alpine Research (INSTAAR) for stable isotopes of CO₂ and CH₄ (Miller et al., 2002;
90 Troler et al., 1996). These samples are also analyzed for a variety of volatile organic compounds
91 (VOCs) including C₂-C₇ NMHCs at INSTAAR since 2004 (Pollmann et al., 2008; Schultz et al.,
92 2015). Since 2014, measurements of ethane and propane were added to discrete air samples
93 collected under the umbrella of the NOAA/GML Halocarbons and other Atmospheric Trace
94 Species (HATS) network since 2004 (<https://www.esrl.noaa.gov/gmd/hats/flask/flasks.html>).

95 The discrete, typically weekly, air sampling by cooperative global networks have been at the
96 forefront of studies to identify and quantify long-term trends in the background air abundances of
97 important trace gases (e.g., Masarie and Tans, 1995; Montzka et al., 2018; Nisbet et al., 2014,
98 2019). In parallel, higher temporal-resolution in-situ measurements allow the investigation of

Deleted: ,

Deleted: and, since 2004,

source regions and of shorter-term trends at specific sites. Here, we report in-situ 2 to 4-hourly ambient air C₂-C₇ NMHCs dry air mole fractions from measurements at the Greenland Environmental Observatory at Summit station (GEOSummit) by gas chromatography (GC) and flame ionization detection (FID). Despite the advent of new methods based on optical measurement (e.g., FTIR spectroscopy) and mass spectrometry (e.g., Photon-Transfer Mass Spectrometry), GC-FID remains the dominant method in routine VOC observations due to its stable long-term response characteristics and relatively low maintenance cost (Schultz et al., 2015). NMHCs were first monitored with high temporal frequency at GEOSummit from 2008 to 2010 with support from the NASA Research Opportunities in Space and Earth Sciences (ROSES) program (Kramer et al., 2015). NMHC monitoring resumed in 2012 as part of the National Science Foundation (NSF) Arctic Observing Network program and has been continuous and uninterrupted until March 2020, providing one of the few high-temporal resolution long-term records of NMHCs in the Arctic. In this paper, we investigate and discuss seasonal variations, rates of change, and potential sources of NMHCs in the high Arctic. We also analyze multiyear trace gas data from other background sites under the umbrella of the NOAA/GML CCGG and HATS sampling networks to support our findings.

2. Materials and Methods

GEOSummit (72.58°N, 38.48°W, 3210 m above sea level) is a research facility located on the Greenland ice sheet funded by the U.S. NSF and operated in collaboration with the Government of Greenland (see Fig. 1). The station hosts a diverse array of Geoscience and Astrophysics research projects (<https://www.geosummit.org/instruments>) and is the only high altitude remote atmospheric observatory in the Arctic. Ambient outside air is monitored at the Temporary Atmospheric Watch Observatory (TAWO), located ~ 1 km south of the research camp.

2.1 In-situ NMHC measurements

C₂-C₇ NMHCs (ethane, propane, iso-butane, n-butane, acetylene, iso-pentane, n-pentane, n-hexane, benzene, toluene) were analyzed from July 2008 to July 2010 and from May 2012 to March 2020 by GC-FID using a fully automated and remotely controlled custom-built system. Ambient air was continuously sampled from a 10 m high inlet on the meteorological tower adjacent to the TAWO building through a heated (~30°C) sampling line. The sampling frequency increased from 6 ambient NMHC runs to 12 daily runs in 2018. The GC-FID system, tailored towards the

Deleted: ,

Deleted: i.e.,

remote, unattended and long-term operation, is a further development of the instrument described in detail by Tanner et al. (2006) and Kramer et al. (2015). The instrument relies on a cryogen-free sample enrichment and injection system. Air was pulled from the tower inlet, and aliquots of the sample stream were first passed through a water trap (u-shaped stainless-steel treated Silcosteel™ tube cooled using thermoelectric coolers) to dry the sample to a dew point of -20°C, and NMHCs were then concentrated on a Peltier-cooled (-35°C) multi-stage adsorbent trap. Analysis was accomplished by thermal desorption and injection onto an Al₂O₃ PLOT column for cryogen-free separation on an SRI Model 8610 GC-FID. Our monitoring effort followed the World Meteorological Organization (WMO) Global Atmospheric Watch (GAW) quality control guidelines: blanks and calibration standards were injected every other day from the manifold and processed in the exact same way as ambient samples. The limit of detection was ~2 ppt (pmol/mol by volume) for all compounds and no significant blank contamination was ever noticed. Quantification was based on monthly FID response factors (Scanlon and Willis, 1985) calculated from the repeated analysis of two independently prepared and cross-referenced standards in use at any given time. Tables S1 and S2 summarize these response factors along with the associated relative standard deviation (< 5 % on average for all compounds) for 2008-2010 and 2012-2020, respectively. The in-situ GC-FID system provided a stable response from 2008 to 2020, with monthly response factors varying by ≤ 5 % for ethane, propane, and butanes, and by ≤ 20 % for other compounds over this period. The monitoring program was audited by the World Calibration Center for Volatile Organic Compounds at the site in July 2017 (<https://www.imk-ifu.kit.edu/wcc-voc/>). All reported VOCs results were found to be within the Global Atmospheric Watch program quality objectives (WMO, 2007).

2.2 Discrete measurements

We use here NMHC data from Alert, Utqiagvik, Mace Head (Ireland), Park Falls (Wisconsin, USA), and Cape Kumukahi (Hawaii, USA; see Fig. 1) collected as part of the NOAA/GML CCGG (October 2004 to August 2016) and HATS (August 2014 to March 2020) sampling and measurement programs. Note that we combine here measurements from the two networks.

2.2.1 CCGG discrete sampling and analysis

As described by Steele et al. (1987) and Dlugokencky et al. (1994), air samples are collected ~weekly in pairs in 2.5 L borosilicate flasks with two glass-piston stopcocks sealed with Teflon O-rings. Flasks are flushed in series for 5 to 10 minutes then pressurized to ~1.2 atm with a portable

165 sampling system. Samples collected from October 2004 to August 2016 were analyzed at
166 INSTAAR in Boulder, Colorado, by GC-FID. The analysis, on a HP-5890 series II gas
167 chromatograph, first involved drying of approximately 600 cubic centimeter (cc) of sample gas by
168 running the sample gas through a 6.4 mm (outer diameter) stainless steel tube cooled to -25°C.
169 The analytes were then preconcentrated at -35°C on an adsorbent bed (Carboxen 1000/1016).
170 Samples were thermally desorbed at 310°C onto a short capillary guard column before separation
171 on an Al₂O₃ PLOT capillary column (0.53 mm × 60 m). Weekly instrument calibrations were
172 performed using primary calibration standards acquired from the NOAA Global Monitoring
173 Laboratory, the U.K. National Physics Laboratory, and the U.S. National Institute of Technology.
174 These standards scales have been maintained since 2006 by regular inter-comparison of standards
175 from these sources and propagation of the scale with newly acquired standards. Deviations in the
176 response factors from these different standards were smaller than 5 %, with results for ethane and
177 propane typically being equal or having less than 2-3 % deviation. Instrument FID response is
178 linear within the range of observed ambient concentrations. The INSTAAR NMHC laboratory was
179 audited by the WMO GAW World Calibration Center for VOCs (WCC-VOC, [https://www.imk-](https://www.imk-ifu.kit.edu/wcc-voc/)
180 [ifu.kit.edu/wcc-voc/](https://www.imk-ifu.kit.edu/wcc-voc/)) in 2008 and in 2016, and both times all measurement results passed the
181 WMO data quality criteria (WMO, 2007).

Deleted: cc

Deleted: o.d.

182 2.2.2 HATS discrete sampling and analysis

183 At GEOSummit, paired borosilicate glass flasks are also pressurized to ~1 atmosphere
184 overpressure with ambient air as part of the HATS sampling program. At other NH sites,
185 electropolished stainless-steel flasks are used. All flasks are analyzed by GC with mass
186 spectrometry analysis with a preconcentration system similar to Miller et al. (2008) to strip water
187 vapor and CO₂ from the airstream prior to injection of condensates (VOCs, halocarbons, solvents,
188 and other gases) onto a 0.32 mm (inner diameter) GasPro capillary column. Results are tied to a
189 suite of standards prepared in-house with gravimetric techniques.

Deleted: i.d.

190 2.3 Ancillary data

191 Continuous monitoring of carbon monoxide (CO) has been ongoing at GEOSummit since May
192 2019 with a cavity ring-down spectroscopy (CRDS) analyzer (Picarro G-2401). A switching
193 manifold allows regular sampling of ambient air and calibration gases. Three NOAA GML
194 standards were integrated into the automated calibration. Low (69.6 ppb) and high (174.6 ppb)
195 calibration points were performed for ~3 minutes every two days, while an intermediate (117.4

199 ppb) calibration was carried out in between. Using the last minute of each calibration, the low and
200 high calibration points were used to determine the linear relationship between the certified
201 calibration values and the analyzer's reported calibration values. The calibration offset (slope and
202 intercept) was calculated and used to correct the third intermediate calibration point. The mean
203 absolute difference between the corrected and certified intermediate calibration paired values was
204 1.6 ppb, *i.e.*, 1.4 %. The minute-averaged CRDS CO ambient air data were corrected using the
205 calibration offset. The CRDS has a manufacturer-specified precision at 5 seconds, 5 minutes, and
206 60 minutes of 15, 1.5, and 1 ppb for CO (G2401 Gas Concentration Analyzer | Picarro, 2020).
207 We also use ethane, propane, tetrachloroethylene (C₂Cl₄), and hydrogen cyanide (HCN) data
208 collected in the free troposphere during the global-scale airborne Atmospheric Tomography
209 mission (ATom; <https://espo.nasa.gov/atom/content/ATom>) onboard the NASA DC-8 aircraft
210 (Wofsy et al., 2018). Canisters collected with the University of California Irvine Whole Air
211 Sampler (WAS) were analyzed for more than 50 trace gases, including ethane, propane, and
212 tetrachloroethylene by GC-FID and GC-mass spectrometric detection (Barletta et al., 2020).
213 Hydrogen cyanide was measured in situ with the California Institute of Technology Chemical
214 Ionization Mass Spectrometer (CIT-CIMS; Allen et al., 2019). For the purpose of our analysis, we
215 removed data collected over continents, in the marine boundary layer (altitude < 0.4 km), or
216 corresponding to stratospheric air (ozone to water vapor ratio > 1 ppb per ppm).

Deleted: filtered out

217 2.4 Curve fitting method and trend analysis

218 We used the curve fitting method developed by Thoning et al. (1989) and described in detail at
219 <https://www.esrl.noaa.gov/gmd/ccgg/mb/krvfit/krvfit.html>. Briefly, the data were fitted with a
220 function consisting of a polynomial and series of harmonics to represent the average long-term
221 trend and seasonal cycle. Residuals from the function were calculated, transformed into frequency
222 domain with a fast Fourier transform algorithm, then filtered with two low pass filters. One
223 eliminates harmonics less than ~1 month. When converted back to time domain and added to the
224 function, it gives a smoothed curve. The other filter eliminates periods less than ~1 year; when
225 transformed back to time domain and added to the polynomial, it gives the deseasonalized trend
226 (hereafter referred to as the trend). The Sen's slope estimate of the trend was calculated using
227 function TheilSen in R package openair (Carslaw and Ropkins, 2012). Note that the p-values and
228 all uncertainties are calculated through bootstrap simulations
229 (<https://davidcarslaw.github.io/openair/reference/TheilSen.html>).

2.5 Source apportionment analysis

In order to identify potential source regions, we performed a Potential Source Contribution Function (PSCF) analysis using the *trajLevel* function in R package *openair* (Carslaw and Ropkins, 2012). Based on air-mass back-trajectories (see below) and NMHC residuals (see Section 2.4), the PSCF calculates the probability that a source is located at latitude i and longitude j . PSCF solves:

$$PSCF = \frac{m_{ij}}{n_{ij}} \quad \text{Eq.1}$$

where n_{ij} is the number of times that the trajectories passed through the cell (i, j) and m_{ij} the number of trajectories passing through that cell in which the NMHC residual was greater than a given threshold (90th percentile of the measured results distribution). Note that cells with very few trajectories passing through them have a weighting factor applied to reduce their effect.

For each NMHC in-situ measurement, HYSPLIT (HYbrid Single Particle Lagrangian Integrated Trajectory; Draxler and Rolph, 2013) 5-day air-mass back trajectories used in the PSCF analysis were generated using the Python package *pysplit* (Warner, 2018) and processor *pysplitprocessor* available at: <https://github.com/brendano257/pysplit> and <https://github.com/brendano257/pysplitprocessor>, respectively. The HYSPLIT Lagrangian particle dispersion model was run from April 2012 to June 2019 using the National Center for Environmental Prediction Global Data Assimilation System (NCEP GDAS) $0.5^\circ \times 0.5^\circ$ meteorological inputs available at: <ftp://arlftp.arlhq.noaa.gov/pub/archives/gdas0p5>. We did not generate back-trajectories for observations after June 2019 due to the unavailability of the GDAS $0.5^\circ \times 0.5^\circ$ archive.

3. Results and Discussion

3.1 Seasonal variation

The seasonal variation of C₂-C₇ NMHCs at GEOSummit is displayed in Fig. 2. Summer refers to June-August, fall to September-November, winter to December-February, and spring to March-May. NMHCs exhibit a strong and consistent seasonal pattern year after year, with maximum mole fractions during winter and early spring, and a rapid decline towards summer. Anthropogenic sources of NMHCs do not vary much seasonally (Pozzer et al., 2010). Therefore, the observed seasonal cycle is primarily driven by the seasonally changing sink strength by the photochemically formed OH radical (Goldstein et al., 1995) – the dominant oxidizing agent in the global troposphere (Levy, 1971; Logan et al., 1981; Thompson, 1992). During the summer period, mole

Deleted: We found a significant correlation ($R^2 = 0.7$, p -value < 0.001) between the mean seasonal amplitude of individual NMHCs and their lifetime against oxidation by the OH radical (Fig. S1).

fractions of the heavier NMHCs were below or close to the GEOSummit in-situ system detection limit (Fig. 2b). As already noted by Goldstein et al. (1995) and Kramer et al. (2015) based on a limited dataset, the phase of each NMHC is shifted due to the rate of reaction with OH. Ethane, the lightest and longest lived of the NMHCs shown in Fig. 2, peaks in February/March with a median of 2110 ppt, and declines to a minimum of 734 ppt in July. Heavier and shorter-lived NMHCs have lower mole fractions, peak earlier in the year (January/February), and reach a minimum earlier in summer (June) due to their faster rate of reaction with OH (Chameides and Cicerone, 1978).

Because changes in NMHC sources and sinks can affect the seasonal cycle amplitude, we investigated whether there is a trend in the NMHC's amplitude at GEOSummit. We focus here on ethane and propane, the most abundant hydrocarbons in the remote atmosphere after methane. Figure 3 shows the amplitude of the ethane and propane seasonal cycles, determined as the relative difference between the maximum and minimum values from the smooth curve for each annual cycle (Dlugokencky et al., 1997). The peak-to-minimum relative amplitude ranged from 64 to 71 % for ethane and from 92 to 96 % for propane, and there is no indication of a significant overall trend in amplitude. This range of amplitudes is in good agreement with the literature: the typical seasonal amplitudes for ethane are on the order of 50 % at mid-latitude sites and can increase up to 80 % at remote sites (Franco et al., 2016; Helmig et al., 2016). Changes in mole fractions are further investigated and discussed in the following section.

3.2 Reversal of ethane and propane rates of change at GEOSummit in 2015

Ethane is released from seepage of fossil carbon deposits, volcanoes, fires, and from human activities – with O&NG extraction, processing, distribution, and industrial use being the primary sources (Pozzer et al., 2010). Based on the inventory developed for the Hemispheric Transport of Air Pollutants, Phase II (HTAP2, Janssens-Maenhout et al., 2015), biogenic emissions from MEGAN2.1 (Guenther et al., 2012), and fire emissions from FINNv1.5 (Wiedinmyer et al., 2011), Helmig et al. (2016) estimated that ~4 %, 18 %, and 78 % of global ethane emissions are due to biogenic, biomass burning, and anthropogenic sources, respectively. Global ethane emission rates decreased by 21 % from 1984 to 2010 likely due to decreased venting and flaring of natural gas in oil producing fields (Simpson et al., 2012). As a consequence, atmospheric ethane background air mixing ratios significantly declined during 1984-2010, by an average of -12.4 ± 1.3 ppt per year in the Northern Hemisphere (Aydin et al., 2011; Worton et al., 2012; Helmig et al., 2014).

297 However, the analysis by Helmig et al. (2016) of ten years (2004-2014) of NMHC data from air
 298 samples collected at NOAA GML remote global sampling sites (including GEOSummit) showed
 299 a reversal of the global ethane trend from mid-2009 to mid-2014 (ethane growth rates > 50 ppt per
 300 year at 32 sites). This trend reversal was attributed to increased U.S. O&NG production (Helmig
 301 et al., 2016). Figure 4a shows the July 2008-March 2020 ethane trend at GEOSummit, as inferred
 302 from our in-situ measurements (dotted line). Note that the same time-series but also showing
 303 individual data points can be found in Fig. S1. Ethane mixing ratios at GEOSummit significantly
 304 (p-value < 0.001) increased by +69.0 [+47.4, +73.2; 95 % confidence interval] ppt per year from
 305 January 2010 to December 2014. A reversal is, however, evident after 2015: ethane mixing ratios
 306 significantly (p-value < 0.001) decreased by -58.4 [-64.1, -48.9] ppt per year from January 2015
 307 to December 2018. Data collected after 2019, however, suggest that the pause in the growth of
 308 atmospheric ethane might only be temporary. We focus hereafter on the 2015-2018 reversal period.
 309 Similar to ethane, a reversal is evident late 2014 for propane (see Fig. 4b; dotted line): mixing
 310 ratios significantly (p-value < 0.001) increased by +47.9 [+32.3, +52.3] ppt per year from January
 311 2010 to June 2014, but significantly (p-value < 0.001) decreased at a rate of -70.5 [-76.1, -65.8]
 312 ppt per year from July 2014 to July 2016. Propane mixing ratios remained fairly stable (+10.2
 313 [+6.6, +14.6] ppt per year; p-value < 0.001) from July 2016 to December 2019. It should be noted
 314 that the pause in the growth of atmospheric ethane and propane at GEOSummit in 2015-2018 is
 315 confirmed by independent discrete sampling under the umbrella of the NOAA/GML CCGG and
 316 HATS networks (see Fig. 4; solid lines). Figure S2 shows the good agreement ($R^2 = 0.97$ for
 317 ethane, $R^2 = 0.99$ for propane) between in-situ GC-FID measurements and discrete samples.
 318 The temporary pause in the growth of ethane and propane at GEOSummit could either suggest
 319 changes in: i) the OH sink strength, ii) atmospheric transport from source regions and/or iii)
 320 natural/anthropogenic emissions.
 321 The tropospheric abundance of OH is driven by a complex series of chemical reactions involving
 322 tropospheric ozone, methane, carbon monoxide, NMHCs, and nitrogen oxides, and by the levels
 323 of solar radiation and humidity (Logan et al., 1981; Thompson, 1992). Building on the comparison
 324 of modeled and observed methane and methyl chloroform lifetimes, Naik et al. (2013) showed that
 325 OH concentrations changed little from 1850 to 2000. The authors suggested that the increases in
 326 factors that enhance OH (humidity, tropospheric ozone, nitrogen oxide emissions, and UV
 327 radiation) was compensated by increases in OH sinks (methane abundance, carbon monoxide and

Deleted: 2

Deleted: year

Deleted: 2

Deleted: a

332 NMHC emissions). More recently, Naus et al. (2020) used a 3D-model inversion of methyl
 333 chloroform to constrain the atmospheric oxidative capacity – largely determined by variations in
 334 OH – for the period 1998-2018. The authors showed that the interannual variations were typically
 335 small (<3 % per year) and found no evidence of a significant long-term trend in OH over the study
 336 period. Changes in NMHC mole fractions at GEOSummit are well outside what could be explained
 337 by a 3% change in OH tropospheric concentrations. There is, however, likely a difference between
 338 global and regional OH variations (Brenninkmeijer et al., 1992; Spivakovsky et al., 2000;
 339 Lelieveld et al., 2004). In the absence of data on the Arctic and mid-latitudes OH abundance, we
 340 concede that OH may play a role on the observed pause but do not discuss that hypothesis further.
 341 The latter two hypotheses are investigated and verified or rejected in the following sections.

342 3.3 **Changes in transport from source regions**

343 The synoptic-scale tropospheric circulation in the Arctic is driven by three major semi-permanent
 344 pressure systems: i) the Aleutian Low, low-pressure center located south of the Bering Sea area,
 345 ii) the Icelandic Low, low-pressure system located southeast of Greenland near Iceland, and iii)
 346 the Siberian High, high-pressure center located over eastern Siberia (Barrie et al., 1992). During
 347 positive phases of the North Atlantic Oscillation (NAO), the Icelandic Low is strengthened and
 348 transport into the Arctic enhanced, resulting in higher Arctic pollution levels (Duncan and Bey,
 349 2004; Eckhardt et al., 2003). Negative phases of the NAO are associated with decreased transport
 350 from Europe and Siberia and increased transport from North America. In addition, mid-latitude
 351 atmospheric blocking events – quasi-stationary features characterized by a high-pressure cell
 352 centered around 60°N and lasting up to ~15 days (Rex, 1950) – are known to enhance transport of
 353 polluted air to the Arctic (Iversen and Joranger, 1985). Here, we test the hypothesis of a pause in
 354 the growth of atmospheric ethane and propane at GEOSummit driven by the interannual variability
 355 of pollution transport from source regions. We investigated the potential influence of the NAO
 356 using monthly mean values from the NOAA Climate Prediction Center. We found a somewhat
 357 weak but significant positive correlation between the NAO and monthly-averaged mixing ratios
 358 over the 2008-2019 period ($R^2 = 0.4$, p-value < 0.01 for both ethane and propane), in line with
 359 enhanced transport of pollution to the Arctic during positive phases of the NAO.

360 Figure 5 shows the origin of air masses influencing GEOSummit (annual gridded back trajectory
 361 frequencies) and Figure 6a summarizes the relative contribution of each geographical sector for
 362 each year. Contrary to other Arctic sites (Hirdman et al., 2010), GEOSummit is mostly influenced

Deleted: No evidence for a change

Deleted: in

Deleted: The interannual variability in the origin of air masses influencing GEOSummit was investigated using April 2012-June 2019 air-mass back trajectories generated with the HYSPLIT model.

Deleted: the

370 by transport from North America and Europe, whereas Siberia has relatively little influence (0-2
371 %). These results are in agreement with the isobaric 10-day back-trajectory study by Kahl et al.
372 (1997) and the 20-day backward FLEXPART simulations by Hirdman et al. (2010). European air
373 masses represented 3-6 % of the total, with a 10 % high in 2018. The relative contribution of North
374 Atlantic air masses (“ocean”) ranged from 1 to 9 %, with a 14 % high from January to August
375 2019. The frequency of North American air masses exhibited the most variability, ranging from 2
376 to 20 %. Years with enhanced transport from North America (e.g., 2012, 2019) coincided with a
377 negative NAO index, known to drive increased transport from North America. Assuming that the
378 ethane and propane trends are driven by emissions in North America (Helmig et al., 2016) and that
379 these emissions are constant, one would expect higher ethane and propane mixing ratios in years
380 when the relative influence of North American air masses peaked. There is, however, an
381 anticorrelation: a 2-3 % relative contribution of North American air masses in 2014 and 2015 when
382 ethane/propane mixing ratios reached a maximum, and 19 % in 2018 when mixing ratios reached
383 a minimum. This leaves two possibilities: either North American emissions dropped over the
384 studied time period (see Section 3.4), or ethane/propane trends observed at GEOSummit are not
385 driven by emissions in North America (see below).

386 The relative contribution of local/regional air masses (i.e., around Greenland, see Fig. 5) increased
387 from 79 % in 2012 to 91-93 % in 2014-2015 before gradually dropping to 61 % in 2018. The
388 apparent correlation between the relative contribution of local/regional air masses and the
389 ethane/propane trend raises the question of whether these are connected. In order to identify
390 potential sources in this sector, we performed a PSCF analysis to investigate source-receptor
391 relationships (e.g., Pekney et al., 2006; Perrone et al., 2018; Yu et al., 2015; Zhou et al., 2018;
392 Zong et al., 2018). The PSCF calculates the probability that a source is located at latitude i and
393 longitude j (Pekney et al., 2006). Figure S3 shows the results of the PSCF analysis for ethane and
394 propane residuals and shows no consistent pattern associated with elevated concentrations. In both
395 winter and summer, the probability of an ethane or propane source from this analysis is low (<2
396 % on average).

397 The history of petroleum exploration activities on the Greenland continental shelf dates back to
398 the 1970s (Arctic Oil & Gas Development: The Case of Greenland, 2020). More recently, the
399 Greenland’s government announced the opening of three new offshore areas for exploration in
400 November 2020 (Greenland Opens Offshore Areas for Drilling, 2020). Despite exploration drilling

Deleted: Local/regional air masses (i.e., around Greenland, see Fig. 5) were the most frequently impacting the site (located near the receptor site). Interestingly,

Deleted: t

Deleted: ir

Deleted: 3

activities, there has never been any O&NG exploitation of Greenland resources (Arctic Oil & Gas Development: The Case of Greenland, 2020). Building on the above, the possibility of a significant local/regional source can be ruled out, and so can the hypothesis that the pause in the growth of ethane and propane is driven by local/regional emissions. The last remaining hypothesis is that this pause is due to a change in emissions from any of the other source sectors, or a combination of them, or total NH emissions and associated change in baseline NH atmospheric levels. This hypothesis is tested in the following Section using observations at other baseline sites.

3.4 Evidence for a hemispheric pattern

Table 1 summarizes the rate of change and 95 % confidence interval for 2010-2014 and 2015-2018 at Alert (ALT, Nunavut, Canada), Utqiagvik/Barrow (BRW, Alaska, USA), Cape Kumukahi (KUM, Hawaii, USA), Park Falls (LEF, Wisconsin, USA), and Mace Head (MHD, Ireland – see Fig. 1) where discrete samples were collected for the NOAA/GML CCGG and HATS cooperative networks. The ethane and propane time-series at the various sites are shown in Figures S4 and S5, respectively. A clear reversal in interannual changes for ethane and propane mixing ratios is observed in 2015 at ALT, BRW, KUM, and LEF. These results support the observed changes at GEOSummit and indicate a hemispheric pattern, likely due to a change in Northern Hemisphere emissions, with a turning point around late 2014. Biomass burning and anthropogenic activities being the main emitters of NMHCs, we hereafter focus the discussion on these two sources.

3.4.1 Biomass burning

Occasional biomass burning plumes were observed at GEOSummit. For example, Fig. 7 shows the simultaneous increase in CO, ethane, propane, and benzene mixing ratios for a short number of days in July and August 2019. According to the Whole Atmosphere Community Climate Model (WACCM; Gettelman et al., 2019) CO forecast simulations, available at <https://www.acom.ucar.edu/waccm/forecast/>, these enhancements can be attributed to intense Siberian wildfires occurring at that time (Bondur et al., 2020). In good agreement with the WACCM simulations, emission ratios (amount of compound emitted divided by that of a reference compound) derived from these two plumes for ethane and propane ($5.4\text{--}5.9 \times 10^{-3}$ and $1.5\text{--}1.6 \times 10^{-3}$ ppb per ppb of CO, respectively; see Fig. S6) are within the range of values reported for boreal forest and peat fires (Andreae, 2019).

Despite the observation of occasional plumes at GEOSummit, the question remains whether biomass burning could drive the observed hemispheric pause in the growth of atmospheric ethane

Deleted: assumption

Deleted: S4

440 and propane. For ethane, the sensitivity to biomass burning emissions from boreal fires is almost
 441 entirely balanced by the larger magnitude of emissions from non-boreal fires (Nicewonger et al.,
 442 2020). Propane being shorter-lived, the fire component over Greenland should be dominated by
 443 emissions from boreal fires. We thus investigate the interannual variability of biomass burning
 444 emissions from both all open burning north of 45°N (boreal fires) and north of the equator (all NH
 445 fires). Figure 6b gives annual biomass burning emissions according to the Fire INventory from
 446 NCAR (FINNv2.2) emission estimates driven by MODIS fire detections (Wiedinmyer et al., in
 447 prep). Emissions north of 45°N peaked in 2012, known for being an exceptional wildfire season
 448 in North America (e.g., Lassman et al., 2017; Val Martin et al., 2013). NH ethane and propane
 449 emissions slightly decreased in 2017 and 2018 but remained fairly stable over the 2008-2016 time
 450 period. We did not find any significant correlation between annual biomass burning emissions and
 451 annually-averaged mixing ratios (true using either 2009-2018 or 2015-2018 data, and true using
 452 either all open burning north of 45°N or north of the equator). The seasonal analysis of the
 453 correlation between ambient air mixing ratios and biomass burning emissions yielded similar
 454 results. This suggests that the observed pause in the growth of atmospheric ethane and propane is
 455 likely not driven by biomass burning emissions.

456 This conclusion is further supported by measurements during the aircraft mission ATom over the
 457 Pacific and Atlantic Oceans. Using ethane and propane data collected in the Northern Hemisphere
 458 (>20°N) remote free troposphere during the four ATom seasonal deployments (July-August 2016,
 459 January-February 2017, September-October 2018, and April-May 2018), we found a significant
 460 positive correlation of ethane and propane with tetrachloroethylene ($R^2 = 0.6$, p-value < 0.001) and
 461 a poor correlation with hydrogen cyanide ($R^2 < 0.1$, p-value < 0.001; see Fig. S7), used as tracers
 462 of anthropogenic and biomass burning emissions, respectively (Bourgeois et al., in review). These
 463 results from the remote free troposphere confirm that atmospheric ethane and propane ambient air
 464 levels are mostly driven by anthropogenic activities rather than by biomass burning emissions, in
 465 line with results from other studies (e.g., Xiao et al., 2008).

3.4.2 O&NG activities

467 Discrete samples collected at northern-hemisphere baseline sites show that the strongest change
 468 was observed at LEF, located downwind from the Bakken oil field in North Dakota (Gvakharia et
 469 al., 2017), with an increase of ethane mixing ratios of +167.7 [+157.5, +186.0] ppt per year in
 470 2010-2014 and a decrease of -247.8 [-312.2, -158.2] ppt per year in 2015-2018 (see Table 1). This

Deleted: from all open burning north of 45°N

Deleted: the contiguous U.S.

Deleted: While

Deleted: remained fairly stable from 2014 to 2018, ethane emissions ...

Deleted: from 2014 to 2016

Deleted: However,

Deleted: we

Deleted: global-scale

Deleted: S5

481 result, along with previous findings by Helmig et al. (2016) and Franco et al. (2015), supports the
482 hypothesis that U.S. O&NG emissions could play a major role in driving atmospheric ethane and
483 propane concentrations in the NH. Here we further discuss this potential contribution to the
484 observed hemispheric pause in the growth of atmospheric ethane and propane in 2015-2018.

485 The U.S. has experienced dramatic increases in O&NG production since 2005, underpinned by
486 technological developments such as horizontal drilling and hydraulic fracturing (Caporin and
487 Fontini, 2017; Feng et al., 2019). This shale revolution has transformed the U.S. into the world's
488 top O&NG producer (Gong, 2020). Coincident with the shale gas boom, the U.S. production of
489 natural gas liquids (ethane, propane, butane, iso-butane, and pentane) has significantly increased
490 in the past decade from 0.6-0.7 billion barrels in the 2000s to 1.1 billion barrels in 2014, and close
491 to 1.8 billion barrels in 2019 (U.S. Field Production of Natural Gas Liquids, 2021). The main
492 source of ethane and propane has been identified to be leakage during the production, processing,
493 and transportation of natural gas (Tzompa-Sosa et al., 2019; Pétron et al., 2012; Roest and Schade,
494 2017).

495 Propane is extracted from natural gas stream and used as a heating fuel. As shown in Figure 8, the
496 U.S. propane field production temporarily plateaued from June 2014 to December 2016 (U.S. Field
497 Production of Propane, 2021) due to a slowdown in natural gas production in response to low
498 natural gas prices. As we consider recent changes in emissions, however, changes in emissions per
499 unit of production must also be considered. A recent study in the Northeastern Colorado Denver-
500 Julesburg Basin showed little change in atmospheric hydrocarbons, including propane, in 2008-
501 2016 despite a 7-fold increase in oil production and nearly tripling of natural gas production,
502 suggesting a significant decrease in leak and/or venting rate per unit of production (Oltmans et al.,
503 2021). While we cannot reliably estimate how propane emissions might have changed during this
504 recent period, these two influences, combined together, could explain the observed temporary
505 pause in the growth of atmospheric propane.

506 Estimating the total production, and ultimately emissions, of ethane is even more complex as it
507 depends on the ethane-to-natural gas price differential. Ethane has long been considered an
508 unwanted byproduct of O&NG drilling, much of it burned away in the natural gas stream or flared
509 off at well sites. Today, ethane is a key feedstock for petrochemical manufacturing and the U.S. is
510 currently the top producer and exporter of ethane (Sicotte, 2020). Depending on the price of ethane
511 relative to natural gas, ethane can be left in the natural gas stream and sold along with natural gas

Deleted: E

Deleted: emissions are

Deleted: primarily due to

Deleted: (Oltmans et al., in review)

516 – a process known as ethane rejection, or separated at natural gas processing plants along with
517 other natural gas liquids (such as propane). Assuming the same leak rates for ethane as for methane,
518 85 % of ethane emissions are due to natural gas extraction and processing, while processed natural
519 gas transportation and use only represent 15 % of the natural gas supply chain ethane loss rate
520 (Alvarez et al., 2018). The slowdown in natural gas production from June 2014 to December 2016
521 (see above) may thus have contributed to the atmospheric ethane plateauing. However, these
522 estimates do not take into account emissions of ethane from its own supply chain (e.g., separation,
523 storage, liquefaction for export, ethane cracker to produce ethylene and plastic resins) – for which
524 leak rates remain unknown. A number of top-down studies, focusing on specific regions or time-
525 periods (e.g., 2010-2014), have shown that current inventories underestimate ethane emissions
526 (e.g., Tzompa-Sosa et al., 2017; Pétron et al., 2014). The modeling study led by Dalsøren et al.
527 (2018) focusing on year 2011 showed that fossil fuel emissions of ethane are likely biased-low by
528 a factor of 2-3. In this highly dynamic context, where ethane production and volume rejected
529 continuously vary and where leak rates change over time (Schwietzke et al., 2014), there is a need
530 for further hemispheric- or global-scale top-down studies focusing on the interannual variability
531 of ethane emissions.

532

533 4. Summary and Conclusion

534 Ethane and propane are the most abundant atmospheric NMHCs and they exert a strong influence
535 on tropospheric ozone, a major air pollutant and greenhouse gas. Increasing levels have been
536 reported in the literature from 2009 to 2014, with evidence pointing at U.S. O&NG activities as
537 the most likely cause (Kort et al., 2016; Helmig et al., 2016; Franco et al., 2016; Hausmann et al.,
538 2016). The long-term high-resolution records of ambient air C₂-C₇ NMHCs at GEOSummit
539 presented here confirm that atmospheric ethane and propane levels increased in the remote arctic
540 troposphere from 2009 to 2015, but also reveal a pause in their growth in 2015-2018. Using
541 independent discrete samples collected at other NH baseline sites, we show that this pause is
542 observed throughout the northern hemisphere – suggesting a change in total NH emissions and in
543 baseline NH atmospheric levels. We further investigated and discussed the contribution of the two
544 main NMHC emitters: biomass burning and O&NG production. We did not find any correlation
545 between atmospheric ethane and propane mixing ratios and the FINNV2.2 biomass burning
546 emission estimates. Additionally, data collected in the NH remote free troposphere during the

Deleted: The analysis of air-mass back-trajectories allowed us to rule out the possibility that this pause is driven by a change in transport from source regions.

ATom aircraft campaign support that atmospheric ethane and propane ambient air levels are mostly driven by anthropogenic activities rather than by biomass burning emissions. The fact that the strongest rate of change reversal was observed at a site located downwind from the Bakken oil field in North Dakota tends to suggest that U.S. O&NG activities yet again played a major role here. The slowdown in U.S. natural gas production from June 2014 to December 2016 combined with a decrease in leak rate per unit of production could have contributed to the observed temporary pause. This conclusion is, however, tentative given the large uncertainties associated with emission estimates, especially with ethane emissions from its supply chain. We hope this work can be used as a starting point to understand what led to the pause in the growth of atmospheric ethane and propane in 2015-2018 and, more generally, to what extent ON&G activities could be responsible for variations in NH baseline ethane and propane levels.

Data availability

All non-methane hydrocarbons and carbon monoxide in-situ data used in this study are archived and publicly available on the Arctic Data Center database (Angot et al., 2020; Helmig, 2017). NOAA/GML HATS and CCGG discrete data are available at <ftp://aftp.cmdl.noaa.gov/data/hats/PERSEUS> and ftp://aftp.cmdl.noaa.gov/data/trace_gases/voc/, respectively.

Author contribution

DH initiated the long-term monitoring effort at GEOSummit and secured funding over the years. JH designed and built the GC-FID used for NMHC in-situ monitoring and performed ~bi-annual on-site visits for maintenance and calibration operations. CD, JC, and BB performed the in-situ data processing (*i.e.*, GC peak identification, peak integration, background subtraction, and calculation of mixing ratios). CD, JC, and HA analyzed the data under the supervision of CW and DH. GP helped evaluating the impact ON&G activities on NMHC trends while IB and CW helped evaluating the impact of biomass burning. IV, SAM, BRM and JWE provided the NOAA /GML HATS discrete data. JH and DH provided the NOAA/GML CCGG NMHC discrete data with contribution from CD, JC, and BB. HA wrote the manuscript with contribution from all co-authors.

Competing interests

581 The authors declare no competing interests.

582

583 **Acknowledgements**

584 We would like to thank the GEOSummit Science Technicians and CH2MHill Polar Services for
585 their tremendous support in enabling on-site and flask collections at the station. HA, JH, and DH
586 would like to acknowledge Maria Soledad Pazos, Miguel Orta Sanchez, and all students involved
587 in the NMHC flask analysis at INSTAAR. IV, SAM, and BRM thank the instrumental analysis
588 assistance of C. Siso and M. Crotwell and standards prepared and maintained by B. Hall at the
589 NOAA GML. We would also like to thank Donald Blake, Paul Wennberg, Michelle Kim, Hannah
590 Allen, John Crounse, and Alex Teng for the ATom dataset used in this analysis.

591

592 **Financial support**

593 The long-term observations and analysis efforts were supported by the [US](#) National Science
594 Foundation (grant nos. 1108391 and 1822406) and the NASA ROSES program (grant no.
595 NNX07AR26G). [HA also received financial support from the Swiss National Science Foundation](#)
596 [\(grant no 200021_188478\)](#). Undergraduate students Connor Davel and Jashan Chopra received
597 financial support from the University of Colorado Boulder's Undergraduate Research
598 Opportunities Program (UROP; grant nos. 7245334 and 5269631, respectively). Support for most
599 CIRES employees is from NOAA award no. NA17OAR4320101. ATom was funded by NASA
600 ROSES-2013 NRA NNH13ZDA001N-EVS2.

601

602 **References**

603 Allen, H. M., Crounse, J. D., Kim, M. J., Teng, A. P., and Wennberg, P. O.: Atmospheric Tomography Mission
604 (ATom)ATom: L2 In Situ Data from Caltech Chemical Ionization Mass Spectrometer (CIT-CIMS), 79.481444 MB,
605 <https://doi.org/10.3334/ORNLDAC/1713>, 2019.

606 Alvarez, R. A., Zavala-Araiza, D., Lyon, D. R., Allen, D. T., Barkley, Z. R., Brandt, A. R., Davis, K. J., Herndon, S.
607 C., Jacob, D. J., Karion, A., Kort, E. A., Lamb, B. K., Lauvaux, T., Maasakkers, J. D., Marchese, A. J., Omara, M.,
608 Pacala, S. W., Peischl, J., Robinson, A. L., Shepson, P. B., Sweeney, C., Townsend-Small, A., Wofsy, S. C., and
609 Hamburg, S. P.: Assessment of methane emissions from the U.S. oil and gas supply chain, 361, 186–188,
610 <https://doi.org/10.1126/science.aar7204>, 2018.

611 Andreae, M. O.: Emission of trace gases and aerosols from biomass burning – an updated assessment, 19, 8523–8546,
612 <https://doi.org/10.5194/acp-19-8523-2019>, 2019.

613 Angot, H., Helmig, D., Hueber, J., Chopra, J., Davel, C., and Wiedinmyer, C.: Atmospheric tracers for Arctic wildfires,
614 air pollution, atmospheric chemistry, and climate change at GEOSummit, Greenland, since 2018,
615 <https://doi.org/10.18739/A2FX73Z7B>, 2020.

616 Aydin, M., Verhulst, K. R., Saltzman, E. S., Battle, M. O., Montzka, S. A., Blake, D. R., Tang, Q., and Prather, M. J.:
617 Recent decreases in fossil-fuel emissions of ethane and methane derived from firm air, *Nature*, 476, 198–201,
618 <https://doi.org/10.1038/nature10352>, 2011.

619 Barletta, B., Biggs, B. C., Blake, D. R., Blake, N., Hoffman, A., Hughes, S., Meinardi, S., Vizenor, N., and Woods,
620 C. T.: ATom: L2 Halocarbons and Hydrocarbons from the UC-Irvine Whole Air Sampler (WAS),
621 <https://doi.org/10.3334/ORNLDAAAC/1751>, 2020.

622 Barrie, L. A., Gregor, D., Hargrave, B., Lake, R., Muir, D., Shearer, R., Tracey, B., and Bidleman, T.: Arctic
623 contaminants: sources, occurrence and pathways, *Science of The Total Environment*, 122, 1–74,
624 [https://doi.org/10.1016/0048-9697\(92\)90245-N](https://doi.org/10.1016/0048-9697(92)90245-N), 1992.

625 Bondur, V. G., Mokhov, I. I., Voronova, O. S., and Sitnov, S. A.: Satellite Monitoring of Siberian Wildfires and Their
626 Effects: Features of 2019 Anomalies and Trends of 20-Year Changes, *Dokl. Earth Sc.*, 492, 370–375,
627 <https://doi.org/10.1134/S1028334X20050049>, 2020.

628 Bourgeois, I., Peischl, J., Neuman, A., Brown, S., Thompson, C., Aikin, K. C., Allen, H. M., Angot, H., Apel, E. C.,
629 Baublitz, C. B., Brewer, J., Campuzano-Jost, P., Commane, R., Crounse, J. D., Daube, B. C., DiGangi, J. P., Diskin,
630 G. S., Emmons, L. K., Fiore, A. M., Gkatzelis, G. I., Hills, A., Hornbrook, R. S., Huey, L. G., Kim, M., Lacey, F.,
631 McKain, L. T., Nault, B. A., Parrish, D. D., Ray, E., Sweeney, C., Tanner, D., Wofsy, S. C., and Ryerson, T. B.: Large
632 contribution of biomass burning emissions to ozone throughout the global remote troposphere, in review.

633 Brenninkmeijer, C. A. M., Manning, M. R., Lowe, D. C., Wallace, G., Sparks, R. J., and Volz-Thomas, A.:
634 Interhemispheric asymmetry in OH abundance inferred from measurements of atmospheric 14 CO, 356, 50–52,
635 <https://doi.org/10.1038/356050a0>, 1992.

636 Caporin, M. and Fontini, F.: The long-run oil–natural gas price relationship and the shale gas revolution, *Energy*
637 *Economics*, 64, 511–519, <https://doi.org/10.1016/j.eneco.2016.07.024>, 2017.

638 Carslaw, D. and Ropkins, K.: openair - An R package for air quality data analysis, *Environ Modell Softw*, 27–28, 52–
639 61, <https://doi.org/10.1016/j.envsoft.2011.09.008>, 2012.

640 Chameides, W. L. and Cicerone, R. J.: EFFECTS OF NONMETHANE HYDROCARBONS IN THE
641 ATMOSPHERE., 83, 947–952, <https://doi.org/10.1029/JC083iC02p00947>, 1978.

642 Dalsøren, S. B., Myhre, G., Hodnebrog, Ø., Myhre, C. L., Stohl, A., Pissio, I., Schwietzke, S., Höglund-Isaksson, L.,
643 Helmig, D., Reimann, S., Sauvage, S., Schmidbauer, N., Read, K. A., Carpenter, L. J., Lewis, A. C., Punjabi, S., and
644 Wallasch, M.: Discrepancy between simulated and observed ethane and propane levels explained by underestimated
645 fossil emissions, 11, 178–184, <https://doi.org/10.1038/s41561-018-0073-0>, 2018.

646 Dlugokencky, E. J., Steele, L. P., Lang, P. M., and Masarie, K. A.: The growth rate and distribution of atmospheric
647 methane, 99, 17021–17043, <https://doi.org/10.1029/94JD01245>, 1994.

648 Dlugokencky, E. J., Masarie, K. A., Tans, P. P., Conway, T. J., and Xiong, X.: Is the amplitude of the methane seasonal
649 cycle changing?, *Atmospheric Environment*, 31, 21–26, [https://doi.org/10.1016/S1352-2310\(96\)00174-4](https://doi.org/10.1016/S1352-2310(96)00174-4), 1997.

650 Draxler, R. R. and Rolph, G. D.: HYSPLIT (HYbrid Single-Particle Lagrangian Integrated Trajectory) Model access
651 via NOAA ARL READY Website (<http://www.arl.noaa.gov/HYSPLIT.php>), last access: 24 October 2015. NOAA
652 Air Resources Laboratory, College Park, MD., 2013.

653 Duncan, B. N. and Bey, I.: A modeling study of the export pathways of pollution from Europe: Seasonal and
654 interannual variations (1987–1997), 109, D08301, <https://doi.org/10.1029/2003JD004079>, 2004.

655 Eckhardt, S., Stohl, A., Beirle, S., Spichtinger, N., James, P., Forster, C., Junker, C., Wagner, T., Platt, U., and
656 Jennings, S. G.: The North Atlantic Oscillation controls air pollution transport to the Arctic, 3, 1769–1778,
657 <https://doi.org/10.5194/acp-3-1769-2003>, 2003.

658 Feng, G.-F., Wang, Q.-J., Chu, Y., Wen, J., and Chang, C.-P.: Does the shale gas boom change the natural gas price-
659 production relationship? Evidence from the U.S. market, *Energy Economics*, 104327,
660 <https://doi.org/10.1016/j.eneco.2019.03.001>, 2019.

661 Franco, B., Bader, W., Toon, G. C., Bray, C., Perrin, A., Fischer, E. V., Sudo, K., Boone, C. D., Bovy, B., Lejeune,
662 B., Servais, C., and Mahieu, E.: Retrieval of ethane from ground-based FTIR solar spectra using improved
663 spectroscopy: Recent burden increase above Jungfraujoch, *Journal of Quantitative Spectroscopy and Radiative*
664 *Transfer*, 160, 36–49, <https://doi.org/10.1016/j.jqsrt.2015.03.017>, 2015.

665 Franco, B., Mahieu, E., Emmons, L. K., Tzompa-Sosa, Z. A., Fischer, E. V., Sudo, K., Bovy, B., Conway, S., Griffin,
666 D., Hannigan, J. W., Strong, K., and Walker, K. A.: Evaluating ethane and methane emissions associated with the
667 development of oil and natural gas extraction in North America, *Environ. Res. Lett.*, 11, 044010,
668 <https://doi.org/10.1088/1748-9326/11/4/044010>, 2016.

669 Geller, L. S., Elkins, J. W., Lobert, J. M., Clarke, A. D., Hurst, D. F., Butler, J. H., and Myers, R. C.: Tropospheric
670 SF₆: Observed latitudinal distribution and trends, derived emissions and interhemispheric exchange time, 24, 675–
671 678, <https://doi.org/10.1029/97GL00523>, 1997.

672 Gettelman, A., Mills, M. J., Kinnison, D. E., Garcia, R. R., Smith, A. K., Marsh, D. R., Tilmes, S., Vitt, F., Bardeen,
673 C. G., McNerny, J., Liu, H.-L., Solomon, S. C., Polvani, L. M., Emmons, L. K., Lamarque, J.-F., Richter, J. H.,
674 Glanville, A. S., Bacmeister, J. T., Phillips, A. S., Neale, R. B., Simpson, I. R., DuVivier, A. K., Hodzic, A., and
675 Randel, W. J.: The Whole Atmosphere Community Climate Model Version 6 (WACCM6), 124, 12380–12403,
676 <https://doi.org/10.1029/2019JD030943>, 2019.

677 Goldstein, A. H., Wofsy, S. C., and Spivakovsky, C. M.: Seasonal variations of nonmethane hydrocarbons in rural
678 New England: Constraints on OH concentrations in northern midlatitudes, 100, 21023–21033,
679 <https://doi.org/10.1029/95JD02034>, 1995.

680 Gong, B.: The Development and Implication of Nature Gas Market in the Context of the Shale Revolution, in: *Shale*
681 *Energy Revolution: The Rise and Fall of Global Oil and Gas Industry*, edited by: Gong, B., Springer, Singapore, 19–
682 36, https://doi.org/10.1007/978-981-15-4855-0_2, 2020.

683 Guenther, A. B., Jiang, X., Heald, C. L., Sakulyanontvittaya, T., Duhl, T., Emmons, L. K., and Wang, X.: The Model
684 of Emissions of Gases and Aerosols from Nature version 2.1 (MEGAN2.1): an extended and updated framework for
685 modeling biogenic emissions, 5, 1471–1492, <https://doi.org/10.5194/gmd-5-1471-2012>, 2012.

686 Gvakharia, A., Kort, E. A., Brandt, A., Peischl, J., Ryerson, T. B., Schwarz, J. P., Smith, M. L., and Sweeney, C.:
687 Methane, Black Carbon, and Ethane Emissions from Natural Gas Flares in the Bakken Shale, North Dakota, *Environ.*
688 *Sci. Technol.*, 51, 5317–5325, <https://doi.org/10.1021/acs.est.6b05183>, 2017.

689 Hartery, S., Commene, R., Lindaas, J., Sweeney, C., Henderson, J., Mountain, M., Steiner, N., McDonald, K., Dinardo,
690 S. J., Miller, C. E., Wofsy, S. C., and Chang, R. Y.-W.: Estimating regional-scale methane flux and budgets using
691 CARVE aircraft measurements over Alaska, 18, 185–202, <https://doi.org/10.5194/acp-18-185-2018>, 2018.

692 Hausmann, P., Sussmann, R., and Smale, D.: Contribution of oil and natural gas production to renewed increase in
693 atmospheric methane (2007–2014): top-down estimate from ethane and methane column observations, 16, 3227–
694 3244, <https://doi.org/10.5194/acp-16-3227-2016>, 2016.

695 Helmig, D.: Atmospheric hydrocarbons as tracers for climate change, air transport, and oxidation chemistry in the
696 Arctic, *GEOSummit, Greenland*, 2008-2017., <https://doi.org/10.18739/A2RS0X>, 2017.

697 Helmig, D., Bottenheim, J., Galbally, I. E., Lewis, A., Milton, M. J. T., Penkett, S., Plass-Duelmer, C., Reimann, S.,
698 Tans, P., and Thiel, S.: Volatile Organic Compounds in the Global Atmosphere, 90, 513–514,
699 <https://doi.org/10.1029/2009EO520001>, 2009.

700 Helmig, D., Petrenko, V., Martinerie, P., Witrant, E., Röckmann, T., Zuiderweg, A., Holzinger, R., Hueber, J.,
701 Thompson, C., White, J. W. C., Sturges, W., Baker, A., Blunier, T., Etheridge, D., Rubino, M., and Tans, P.:
702 Reconstruction of Northern Hemisphere 1950–2010 atmospheric non-methane hydrocarbons, 14, 1463–1483,
703 <https://doi.org/10.5194/acp-14-1463-2014>, 2014.

704 Helmig, D., Rossabi, S., Hueber, J., Tans, P., Montzka, S. A., Masarie, K., Thoning, K., Plass-Duelmer, C., Claude,
705 A., Carpenter, L. J., Lewis, A. C., Punjabi, S., Reimann, S., Vollmer, M. K., Steinbrecher, R., Hannigan, J. W.,
706 Emmons, L. K., Mahieu, E., Franco, B., Smale, D., and Pozzer, A.: Reversal of global atmospheric ethane and propane
707 trends largely due to US oil and natural gas production, 9, 490–495, <https://doi.org/10.1038/ngeo2721>, 2016.

708 Hirdman, D., Sodemann, H., Eckhardt, S., Burkhardt, J. F., Jefferson, A., Mefford, T., Quinn, P. K., Sharma, S., Ström,
709 J., and Stohl, A.: Source identification of short-lived air pollutants in the Arctic using statistical analysis of
710 measurement data and particle dispersion model output, 10, 669–693, <https://doi.org/10.5194/acp-10-669-2010>, 2010.

711 Houweling, S., Dentener, F., and Lelieveld, J.: The impact of nonmethane hydrocarbon compounds on tropospheric
712 photochemistry, 103, 10673–10696, <https://doi.org/10.1029/97JD03582>, 1998.

713 Iversen, T. and Joranger, E.: Arctic air pollution and large scale atmospheric flows, *Atmospheric Environment* (1967),
714 19, 2099–2108, [https://doi.org/10.1016/0004-6981\(85\)90117-9](https://doi.org/10.1016/0004-6981(85)90117-9), 1985.

715 Jacob, D. J., Crawford, J. H., Maring, H., Clarke, A. D., Dibb, J. E., Emmons, L. K., Ferrare, R. A., Hostetler, C. A.,
716 Russell, P. B., Singh, H. B., Thompson, A. M., Shaw, G. E., McCauley, E., Pederson, J. R., and Fisher, J. A.: The
717 Arctic Research of the Composition of the Troposphere from Aircraft and Satellites (ARCTAS) mission: design,
718 execution, and first results, 10, 5191–5212, <https://doi.org/10.5194/acp-10-5191-2010>, 2010.

719 Janssens-Maenhout, G., Crippa, M., Guizzardi, D., Dentener, F., Muntean, M., Pouliot, G., Keating, T., Zhang, Q.,
720 Kurokawa, J., Wankmüller, R., Denier van der Gon, H., Kuenen, J. J. P., Klimont, Z., Frost, G., Darras, S., Koffi, B.,
721 and Li, M.: HTAP_v2.2: a mosaic of regional and global emission grid maps for 2008 and 2010 to study hemispheric
722 transport of air pollution, 15, 11411–11432, <https://doi.org/10.5194/acp-15-11411-2015>, 2015.

723 Kahl, J. D. W., Martinez, D. A., Kuhns, H., Davidson, C. I., Jaffrezo, J.-L., and Harris, J. M.: Air mass trajectories to
724 Summit, Greenland: A 44-year climatology and some episodic events, 102, 26861–26875,
725 <https://doi.org/10.1029/97JC00296>, 1997.

726 Komhyr, W. D., Gammon, R. H., Harris, T. B., Waterman, L. S., Conway, T. J., Taylor, W. R., and Thoning, K. W.:
727 Global atmospheric CO₂ distribution and variations from 1968–1982 NOAA/GMCC CO₂ flask sample data, 90,
728 5567–5596, <https://doi.org/10.1029/JD090iD03p05567>, 1985.

729 Kort, E. A., Smith, M. L., Murray, L. T., Gvakharia, A., Brandt, A. R., Peischl, J., Ryerson, T. B., Sweeney, C., and
730 Travis, K.: Fugitive emissions from the Bakken shale illustrate role of shale production in global ethane shift, 43,
731 4617–4623, <https://doi.org/10.1002/2016GL068703>, 2016.

732 Kramer, L. J., Helmig, D., Burkhardt, J. F., Stohl, A., Oltmans, S., and Honrath, R. E.: Seasonal variability of
733 atmospheric nitrogen oxides and non-methane hydrocarbons at the GEOSummit station, Greenland, 15, 6827–6849,
734 <https://doi.org/10.5194/acp-15-6827-2015>, 2015.

735 Lassman, W., Ford, B., Gan, R. W., Pfister, G., Magzamen, S., Fischer, E. V., and Pierce, J. R.: Spatial and temporal
736 estimates of population exposure to wildfire smoke during the Washington state 2012 wildfire season using blended
737 model, satellite, and in situ data, 1, 106–121, <https://doi.org/10.1002/2017GH000049>, 2017.

738 Law, K. S., Stohl, A., Quinn, P. K., Brock, C., Burkhardt, J., Paris, J.-D., Ancellet, G., Singh, H. B., Roiger, A.,
739 Schlager, H., Dibb, J., Jacob, D. J., Arnold, S. R., Pelon, J., and Thomas, J. L.: Arctic Air Pollution: New Insights
740 from POLARCAT-IPY, <https://doi.org/10.1175/BAMS-D-13-00017.1>, 2014.

741 Lelieveld, J., Dentener, F. J., Peters, W., and Krol, M. C.: On the role of hydroxyl radicals in the self-cleansing capacity
742 of the troposphere, 4, 2337–2344, <https://doi.org/10.5194/acp-4-2337-2004>, 2004.

743 Levy, H.: Normal Atmosphere: Large Radical and Formaldehyde Concentrations Predicted, 173, 141–143,
744 <https://doi.org/10.1126/science.173.3992.141>, 1971.

745 Logan, J. A., Prather, M. J., Wofsy, S. C., and McElroy, M. B.: Tropospheric chemistry: A global perspective, 86,
746 7210–7254, <https://doi.org/10.1029/JC086iC08p07210>, 1981.

747 Masarie, K. A. and Tans, P. P.: Extension and integration of atmospheric carbon dioxide data into a globally consistent
748 measurement record, 100, 11593–11610, <https://doi.org/10.1029/95JD00859>, 1995.

749 Miller, B. R., Weiss, R. F., Salameh, P. K., Tanhua, T., Grealley, B. R., Mühle, J., and Simmonds, P. G.: Medusa: A
750 Sample Preconcentration and GC/MS Detector System for in Situ Measurements of Atmospheric Trace Halocarbons,
751 Hydrocarbons, and Sulfur Compounds, *Anal. Chem.*, 80, 1536–1545, <https://doi.org/10.1021/ac702084k>, 2008.

752 Miller, J. B., Mack, K. A., Dissly, R., White, J. W. C., Dlugokencky, E. J., and Tans, P. P.: Development of analytical
753 methods and measurements of $^{13}\text{C}/^{12}\text{C}$ in atmospheric CH_4 from the NOAA Climate Monitoring and Diagnostics
754 Laboratory Global Air Sampling Network, 107, ACH 11-1-ACH 11-15, <https://doi.org/10.1029/2001JD000630>, 2002.

755 Montzka, S. A., Dutton, G. S., Yu, P., Ray, E., Portmann, R. W., Daniel, J. S., Kuijpers, L., Hall, B. D., Mondeel, D.,
756 Siso, C., Nance, J. D., Rigby, M., Manning, A. J., Hu, L., Moore, F., Miller, B. R., and Elkins, J. W.: An unexpected
757 and persistent increase in global emissions of ozone-depleting CFC-11, 557, 413–417, [https://doi.org/10.1038/s41586-](https://doi.org/10.1038/s41586-018-0106-2)
758 018-0106-2, 2018.

759 Naik, V., Voulgarakis, A., Fiore, A. M., Horowitz, L. W., Lamarque, J.-F., Lin, M., Prather, M. J., Young, P. J.,
760 Bergmann, D., Cameron-Smith, P. J., Cionni, I., Collins, W. J., Dalsøren, S. B., Doherty, R., Eyring, V., Faluvegi, G.,
761 Folberth, G. A., Josse, B., Lee, Y. H., MacKenzie, I. A., Nagashima, T., van Noije, T. P. C., Plummer, D. A., Righi,
762 M., Rumbold, S. T., Skeie, R., Shindell, D. T., Stevenson, D. S., Strode, S., Sudo, K., Szopa, S., and Zeng, G.:
763 Preindustrial to present-day changes in tropospheric hydroxyl radical and methane lifetime from the Atmospheric
764 Chemistry and Climate Model Intercomparison Project (ACCMIP), 13, 5277–5298, [https://doi.org/10.5194/acp-13-](https://doi.org/10.5194/acp-13-5277-2013)
765 5277-2013, 2013.

766 Naus, S., Montzka, S. A., Patra, P. K., and Krol, M. C.: A 3D-model inversion of methyl chloroform to constrain the
767 atmospheric oxidative capacity, 1–23, <https://doi.org/10.5194/acp-2020-624>, 2020.

768 Nicewonger, M. R., Aydin, M., Prather, M. J., and Saltzman, E. S.: Extracting a History of Global Fire Emissions for
769 the Past Millennium From Ice Core Records of Acetylene, Ethane, and Methane, 125, e2020JD032932,
770 <https://doi.org/10.1029/2020JD032932>, 2020.

771 Nisbet, E. G., Dlugokencky, E. J., and Bousquet, P.: Methane on the Rise—Again, 343, 493–495,
772 <https://doi.org/10.1126/science.1247828>, 2014.

773 Nisbet, E. G., Manning, M. R., Dlugokencky, E. J., Fisher, R. E., Lowry, D., Michel, S. E., Myhre, C. L., Platt, S. M.,
774 Allen, G., Bousquet, P., Brownlow, R., Cain, M., France, J. L., Hermansen, O., Hossaini, R., Jones, A. E., Levin, I.,
775 Manning, A. C., Myhre, G., Pyle, J. A., Vaughn, B. H., Warwick, N. J., and White, J. W. C.: Very Strong Atmospheric
776 Methane Growth in the 4 Years 2014–2017: Implications for the Paris Agreement, 33, 318–342,
777 <https://doi.org/10.1029/2018GB006009>, 2019.

778 Oltmans, S. J., Cheadle, L. C., Helmig, D., Angot, H., Pétron, G., Montzka, S. A., Dlugokencky, E. J., Miller, B., Hall,
779 B., Schnell, R. C., Kofler, J., Wolter, S., Crotwell, M., Siso, C., Tans, P., and Andrews, A.: Atmospheric oil and

780 natural gas hydrocarbon trends in the Northern Colorado Front Range are notably smaller than inventory emissions
781 reductions, *Elementa: Science of the Anthropocene*, 9, <https://doi.org/10.1525/elementa.2020.00136>, 2021.

782 Pekney, N. J., Davidson, C. I., Zhou, L., and Hopke, P. K.: Application of PSCF and CPF to PMF-Modeled Sources
783 of PM_{2.5} in Pittsburgh, 40, 952–961, <https://doi.org/10.1080/02786820500543324>, 2006.

784 Perrone, M. G., Vratolis, S., Georgieva, E., Török, S., Šega, K., Veleva, B., Osán, J., Bešlić, I., Kertész, Z., Pernigotti,
785 D., Eleftheriadis, K., and Belis, C. A.: Sources and geographic origin of particulate matter in urban areas of the Danube
786 macro-region: The cases of Zagreb (Croatia), Budapest (Hungary) and Sofia (Bulgaria), *Sci Total Environ*, 619–620,
787 1515–1529, <https://doi.org/10.1016/j.scitotenv.2017.11.092>, 2018.

788 Pétron, G., Frost, G., Miller, B. R., Hirsch, A. I., Montzka, S. A., Karion, A., Trainer, M., Sweeney, C., Andrews, A.
789 E., Miller, L., Kofler, J., Bar-Ilan, A., Dlugokencky, E. J., Patrick, L., Moore, C. T., Ryerson, T. B., Siso, C., Kolodzey,
790 W., Lang, P. M., Conway, T., Novelli, P., Masarie, K., Hall, B., Guenther, D., Kitzis, D., Miller, J., Welsh, D., Wolfe,
791 D., Neff, W., and Tans, P.: Hydrocarbon emissions characterization in the Colorado Front Range: A pilot study, 117,
792 <https://doi.org/10.1029/2011JD016360>, 2012.

793 Pétron, G., Karion, A., Sweeney, C., Miller, B. R., Montzka, S. A., Frost, G. J., Trainer, M., Tans, P., Andrews, A.,
794 Helmig, J., Helmig, D., Guenther, D., Dlugokencky, E., Lang, P., Newberger, T., Wolter, S., Hall, B., Novelli, P.,
795 Brewer, A., Conley, S., Hardesty, M., Banta, R., White, A., Noone, D., Wolfe, D., and Schnell, R.: A new look at
796 methane and nonmethane hydrocarbon emissions from oil and natural gas operations in the Colorado Denver-
797 Julesburg Basin, 119, 6836–6852, <https://doi.org/10.1002/2013JD021272>, 2014.

798 G2401 Gas Concentration Analyzer | Picarro: https://www.picarro.com/products/g2401_gas_concentration_analyzer,
799 last access: 31 March 2020.

800 Pollmann, J., Helmig, D., Hueber, J., Plass-Dülmer, C., and Tans, P.: Sampling, storage, and analysis of C₂–C₇ non-
801 methane hydrocarbons from the US National Oceanic and Atmospheric Administration Cooperative Air Sampling
802 Network glass flasks, *Journal of Chromatography A*, 1188, 75–87, <https://doi.org/10.1016/j.chroma.2008.02.059>,
803 2008.

804 Arctic Oil & Gas Development: The Case of Greenland: [https://arcticyearbook.com/arctic-yearbook/2018/2018-](https://arcticyearbook.com/arctic-yearbook/2018/2018-scholarly-papers/285-arctic-oil-gas-development-the-case-of-greenland)
805 [scholarly-papers/285-arctic-oil-gas-development-the-case-of-greenland](https://arcticyearbook.com/arctic-yearbook/2018/2018-scholarly-papers/285-arctic-oil-gas-development-the-case-of-greenland), last access: 25 November 2020.

806 Pozzer, A., Pollmann, J., Taraborrelli, D., Jöckel, P., Helmig, D., Tans, P., Hueber, J., and Lelieveld, J.: Observed and
807 simulated global distribution and budget of atmospheric C₂–C₅ alkanes, 10, 4403–4422, [https://doi.org/10.5194/acp-](https://doi.org/10.5194/acp-10-4403-2010)
808 [10-4403-2010](https://doi.org/10.5194/acp-10-4403-2010), 2010.

809 Rex, D. F.: Blocking Action in the Middle Troposphere and its Effect upon Regional Climate, 2, 275–301,
810 <https://doi.org/10.1111/j.2153-3490.1950.tb00339.x>, 1950.

811 Greenland Opens Offshore Areas for Drilling:
812 https://www.rigzone.com/news/greenland_opens_offshore_areas_for_drilling-05-nov-2020-163772-article/, last
813 access: 25 November 2020.

814 Roest, G. and Schade, G.: Quantifying alkane emissions in the Eagle Ford Shale using boundary layer enhancement,
815 17, 11163–11176, <https://doi.org/10.5194/acp-17-11163-2017>, 2017.

816 Rudolph, J.: The tropospheric distribution and budget of ethane, 100, 11369–11381,
817 <https://doi.org/10.1029/95JD00693>, 1995.

818 Scanlon, J. T. and Willis, D. E.: Calculation of Flame Ionization Detector Relative Response Factors Using the
819 Effective Carbon Number Concept, *J Chromatogr Sci*, 23, 333–340, <https://doi.org/10.1093/chromsci/23.8.333>, 1985.

820 von Schneidmesser, E., Monks, P. S., and Plass-Duelmer, C.: Global comparison of VOC and CO observations in
821 urban areas, *Atmospheric Environment*, 44, 5053–5064, <https://doi.org/10.1016/j.atmosenv.2010.09.010>, 2010.

822 Schultz, M. G., Akimoto, H., Bottenheim, J., Buchmann, B., Galbally, I. E., Gilge, S., Helmig, D., Koide, H., Lewis,
823 A. C., Novelli, P. C., Dülmer, C. P., Ryerson, T. B., Steinbacher, M., Steinbrecher, R., Tarasova, O., Tørseth, K.,
824 Thouret, V., and Zellweger, C.: The Global Atmosphere Watch reactive gases measurement network, 3, 000067,
825 <https://doi.org/10.12952/journal.elementa.000067>, 2015.

826 Sicotte, D. M.: From cheap ethane to a plastic planet: Regulating an industrial global production network, *Energy*
827 *Research & Social Science*, 66, 101479, <https://doi.org/10.1016/j.erss.2020.101479>, 2020.

828 Simpson, I. J., Andersen, M. P. S., Meinardi, S., Bruhwiler, L., Blake, N. J., Helmig, D., Rowland, F. S., and Blake,
829 D. R.: Long-term decline of global atmospheric ethane concentrations and implications for methane, *Nature*, 488,
830 490–494, <https://doi.org/10.1038/nature11342>, 2012.

831 Spivakovsky, C. M., Logan, J. A., Montzka, S. A., Balkanski, Y. J., Foreman-Fowler, M., Jones, D. B. A., Horowitz,
832 L. W., Fusco, A. C., Brenninkmeijer, C. a. M., Prather, M. J., Wofsy, S. C., and McElroy, M. B.: Three-dimensional
833 climatological distribution of tropospheric OH: Update and evaluation, 105, 8931–8980,
834 <https://doi.org/10.1029/1999JD901006>, 2000.

835 Steele, L. P.: Atmospheric Methane Concentrations, the NOAA/CMDL Global Cooperative Flask Sampling Network,
836 1983–1988, Oak Ridge National Laboratory, 324 pp., 1991.

837 Steele, L. P., Fraser, P. J., Rasmussen, R. A., Khalil, M. A. K., Conway, T. J., Crawford, A. J., Gammon, R. H.,
838 Masarie, K. A., and Thoning, K. W.: The global distribution of methane in the troposphere, *J Atmos Chem*, 5, 125–
839 171, <https://doi.org/10.1007/BF00048857>, 1987.

840 Tanner, D., Helmig, D., Hueber, J., and Goldan, P.: Gas chromatography system for the automated, unattended, and
841 cryogen-free monitoring of C2 to C6 non-methane hydrocarbons in the remote troposphere, *Journal of*
842 *Chromatography A*, 1111, 76–88, <https://doi.org/10.1016/j.chroma.2006.01.100>, 2006.

843 Thompson, A. M.: The Oxidizing Capacity of the Earth’s Atmosphere: Probable Past and Future Changes, 256, 1157–
844 1165, <https://doi.org/10.1126/science.256.5060.1157>, 1992.

845 Thoning, K. W., Tans, P. P., and Komhyr, W. D.: Atmospheric carbon dioxide at Mauna Loa Observatory: 2. Analysis
846 of the NOAA GMCC data, 1974–1985, 94, 8549–8565, <https://doi.org/10.1029/JD094iD06p08549>, 1989.

847 Trolier, M., White, J. W. C., Tans, P. P., Masarie, K. A., and Gemery, P. A.: Monitoring the isotopic composition of
848 atmospheric CO₂: Measurements from the NOAA Global Air Sampling Network, 101, 25897–25916,
849 <https://doi.org/10.1029/96JD02363>, 1996.

850 Tzompa-Sosa, Z. A., Mahieu, E., Franco, B., Keller, C. A., Turner, A. J., Helmig, D., Fried, A., Richter, D., Weibring,
851 P., Walega, J., Yacovitch, T. I., Herndon, S. C., Blake, D. R., Hase, F., Hannigan, J. W., Conway, S., Strong, K.,
852 Schneider, M., and Fischer, E. V.: Revisiting global fossil fuel and biofuel emissions of ethane, 122, 2493–2512,
853 <https://doi.org/10.1002/2016JD025767>, 2017.

854 Tzompa-Sosa, Z. A., Henderson, B. H., Keller, C. A., Travis, K., Mahieu, E., Franco, B., Estes, M., Helmig, D., Fried,
855 A., Richter, D., Weibring, P., Walega, J., Blake, D. R., Hannigan, J. W., Ortega, I., Conway, S., Strong, K., and
856 Fischer, E. V.: Atmospheric Implications of Large C₂-C₅ Alkane Emissions From the U.S. Oil and Gas Industry, 124,
857 1148–1169, <https://doi.org/10.1029/2018JD028955>, 2019.

858 U.S. Field Production of Natural Gas Liquids:
859 https://www.eia.gov/dnav/pet/hist/LeafHandler.ashx?n=PET&s=M_EPL2_FPF_NUS_MBBLD&f=A, last access: 8
860 March 2021.

861 U.S. Field Production of Propane:
862 https://www.eia.gov/dnav/pet/hist/LeafHandler.ashx?n=PET&s=M_EPLLP_FPF_NUS_MBBL&f=M, last access:
863 8 March 2021.

864 Val Martin, M., Heald, C. L., Ford, B., Prenni, A. J., and Wiedinmyer, C.: A decadal satellite analysis of the origins
865 and impacts of smoke in Colorado, 2013.

866 Warneke, C., Gouw, J. A. de, Holloway, J. S., Peischl, J., Ryerson, T. B., Atlas, E., Blake, D., Trainer, M., and Parrish,
867 D. D.: Multiyear trends in volatile organic compounds in Los Angeles, California: Five decades of decreasing
868 emissions, 117, <https://doi.org/10.1029/2012JD017899>, 2012.

869 Warner, M. S. C.: Introduction to PySPLIT: A Python Toolkit for NOAA ARL's HYSPLIT Model, 20, 47–62,
870 <https://doi.org/10.1109/MCSE.2017.3301549>, 2018.

871 Wiedinmyer, C., Akagi, S. K., Yokelson, R. J., Emmons, L. K., Al-Saadi, J. A., Orlando, J. J., and Soja, A. J.: The
872 Fire INventory from NCAR (FINN): a high resolution global model to estimate the emissions from open burning, 4,
873 625–641, <https://doi.org/10.5194/gmd-4-625-2011>, 2011.

874 Wiedinmyer, C., Kumra, Y., McDonald-Buller, E. C., Seto, K., Emmons, L. K., Buccholz, R., Tang, W., Joseph, M.,
875 Barsanti, K., Carlton, A. M., and Yokelson, R. J.: The Fire Inventory from NCAR version 2: an updated global fire
876 emissions model for climate and chemistry applications., *Journal of Advances in Modeling Earth Systems*, in prep.

877 WMO: GAW Report, 171. A WMO/GAW Expert Workshop on Global Long-term Measurements of Volatile Organic
878 Compounds, WMO, Geneva, 36 p. pp., 2007.

879 Wofsy, S. C., Afshar, S., Allen, H. M., Apel, E. C., Asher, E. C., Barletta, B., Bent, J., Bian, H., Biggs, B. C., Blake,
880 D. R., Blake, N., Bourgeois, I., Brock, C. A., Brune, W. H., Budney, J. W., Bui, T. P., Butler, A., Campuzano-Jost,
881 P., Chang, C. S., Chin, M., Commance, R., Correa, G., Crounse, J. D., Cullis, P. D., Daube, B. C., Day, D. A., Dean-
882 Day, J. M., Dibb, J. E., Digangi, J. P., Diskin, G. S., Dollner, M., Elkins, J. W., Erdesz, F., Fiore, A. M., Flynn, C. M.,
883 Froyd, K. D., Gesler, D. W., Hall, S. R., Hanisco, T. F., Hannun, R. A., Hills, A. J., Hints, E. J., Hoffman, A.,
884 Hornbrook, R. S., Huey, L. G., Hughes, S., Jimenez, J. L., Johnson, B. J., Katich, J. M., Keeling, R. F., Kim, M. J.,
885 Kupc, A., Lait, L. R., Lamarque, J.-F., Liu, J., Mckain, K., McLaughlin, R. J., Meinardi, S., Miller, D. O., Montzka, S.
886 A., Moore, F. L., Morgan, E. J., Murphy, D. M., Murray, L. T., Nault, B. A., Neuman, J. A., Newman, P. A., Nicely,
887 J. M., Pan, X., Paplawsky, W., Peischl, J., Prather, M. J., Price, D. J., Ray, E. A., Reeves, J. M., Richardson, M.,
888 Rollins, A. W., Rosenlof, K. H., Ryerson, T. B., Scheuer, E., Schill, G. P., Schroder, J. C., Schwarz, J. P., St. Clair, J.
889 M., Steenrod, S. D., Stephens, B. B., Strode, S. A., Sweeney, C., Tanner, D., Teng, A. P., Thames, A. B., Thompson,
890 C. R., Ullmann, K., Veres, P. R., Vizenor, N., Wagner, N. L., Watt, A., Weber, R., Weinzierl, B., et al.: ATom: Merged
891 Atmospheric Chemistry, Trace Gases, and Aerosols, <https://doi.org/10.3334/ORNLDAAAC/1581>, 2018.

892 Worton, D. R., Sturges, W. T., Reeves, C. E., Newland, M. J., Penkett, S. A., Atlas, E., Stroud, V., Johnson, K.,
893 Schmidbauer, N., Solberg, S., Schwander, J., and Barnola, J.-M.: Evidence from firn air for recent decreases in non-
894 methane hydrocarbons and a 20th century increase in nitrogen oxides in the northern hemisphere, *Atmospheric*
895 *Environment*, 54, 592–602, <https://doi.org/10.1016/j.atmosenv.2012.02.084>, 2012.

896 Xiao, Y., Logan, J. A., Jacob, D. J., Hudman, R. C., Yantosca, R., and Blake, D. R.: Global budget of ethane and
897 regional constraints on U.S. sources, 113, <https://doi.org/10.1029/2007JD009415>, 2008.

898 Yu, Y., Hung, H., Alexandrou, N., Roach, P., and Nordin, K.: Multiyear Measurements of Flame Retardants and
899 Organochlorine Pesticides in Air in Canada's Western Sub-Arctic, *Environ. Sci. Technol.*, 49, 8623–8630,
900 <https://doi.org/10.1021/acs.est.5b01996>, 2015.

901 Zhou, H., Hopke, P. K., Zhou, C., and Holsen, T. M.: Ambient mercury source identifications at a New York State
902 urban site: Rochester, NY, *Science of The Total Environment*, <https://doi.org/10.1016/j.scitotenv.2018.09.040>, 2018.

903 Zong, Z., Wang, X., Tian, C., Chen, Y., Fu, S., Qu, L., Ji, L., Li, J., and Zhang, G.: PMF and PSCF based source
904 apportionment of PM_{2.5} at a regional background site in North China, *Atmospheric Research*, 203, 207–215,
905 <https://doi.org/10.1016/j.atmosres.2017.12.013>, 2018.

Table 1: Rates of change and 95 % confidence interval (in brackets) inferred from discrete flask sampling (in ppt per year). ALT, BRW, MHD, LEF, and KUM refer to Alert, Utqiagvik/Barrow, Mace Head, Park Falls, and Cape Kumukahi. The localization of the sites can be found in Figure 1. The symbols shown next to each rate of change relate to how statistically significant the estimate is: $p < 0.001 = ***$, $p < 0.01 = **$, and $p < 0.05 = *$.

Site	2010-2014	2015-2018
Ethane		
ALT	+52.8 [+32.7, +73.0] ***	-56.9 [-79.9, -36.6] ***
BRW	+40.5 [+25.9, +59.1] ***	-50.6 [-69.4, -27.6] ***
KUM	+18.4 [+7.9, +29.5] ***	-43.1 [-62.1, -28.1] ***
LEF	+167.7 [+157.5, +186.0] ***	-247.8 [-312.2, -158.2] ***
MHD	+51.8 [+44.4, +63.2] ***	-18.6 [-102.6, +45.4]
Propane		
ALT	+24.8 [+16.5, +37.7] ***	-55.6 [-65.1, -45.9] ***
BRW	+14.5 [+9.1, +20.2] ***	-35.1 [-45.3, -25.6] ***
KUM	+3.1 [+0.2, +5.9] *	-13.2 [-15.9, -10.7] ***
LEF	+89.8 [+68.5, +123.5] ***	-110.0 [-173.6, -75.6] ***
MHD	+21.3 [+16.9, +27.1] ***	-24.2 [-56.2, -7.2] **

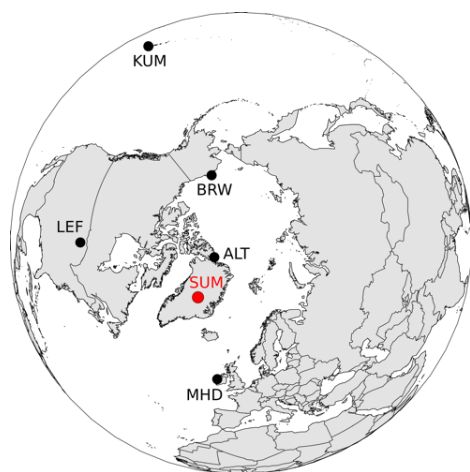


Figure 1: Location of the Greenland Environmental Observatory at Summit station (red dot, SUM) where long-term in-situ monitoring was carried out, and of Alert (ALT), Utqiagvik (formerly known as Barrow (BRW)), Mace Head (MHD), Park Falls (LEF), and Cape Kumukahi (KUM) where discrete samples were collected by both the NOAA/ESRL/GML CCGG and HATS flask sampling programs. The map is centered over the North Pole.

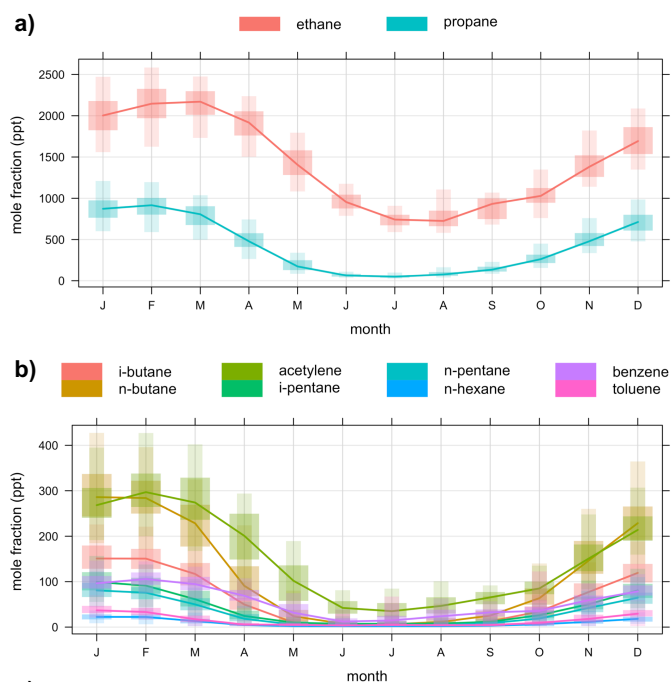


Figure 2: Monthly variation of **a)** ethane and propane, and **b)** C4-C7 non-methane hydrocarbons measured in ambient air at GEOSummit as inferred from 2008-2010 and 2012-2020 in-situ measurements. In the monthly boxplots, the lower and upper end of the box correspond to the 25th and 75th percentiles while the whiskers extend from the 5th to the 95th percentiles.

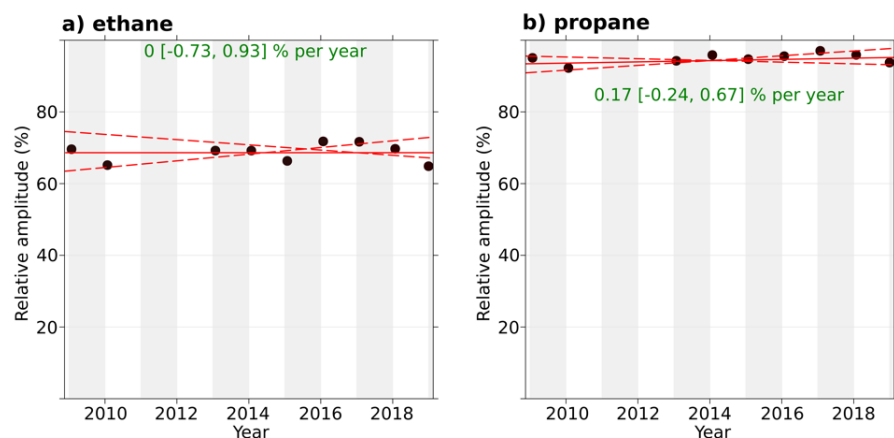


Figure 3: Trend in peak-to-peak seasonal amplitude of **a)** ethane and **b)** propane at GEOSummit, calculated as the relative difference between the maximum and minimum values from the smooth curve for each annual cycle. The solid red line shows the trend estimate and the dashed red lines show the 95 % confidence interval for the trend based on resampling methods. The overall trend is shown at the top along with the 95 % confidence interval in the slope.

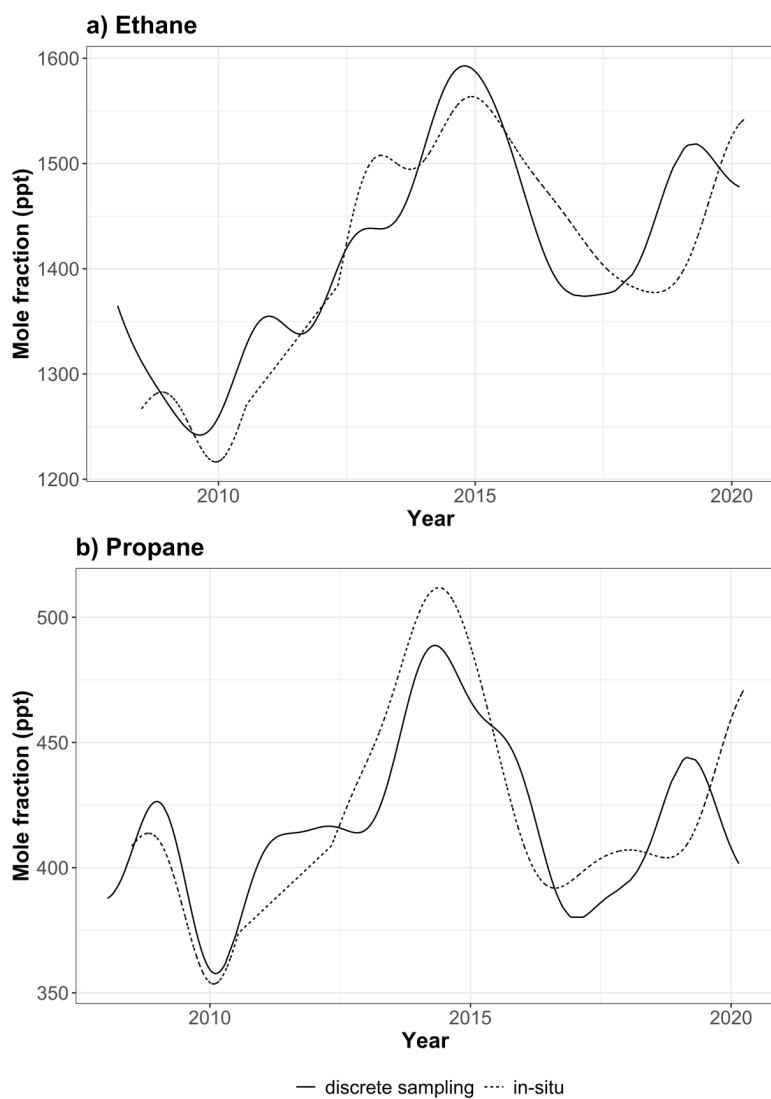


Figure 4: a) Ethane, and b) propane trends at GEOSummit from July 2008 to March 2020. Trends inferred from in-situ and discrete flask sampling are shown by the dotted and solid lines, respectively.

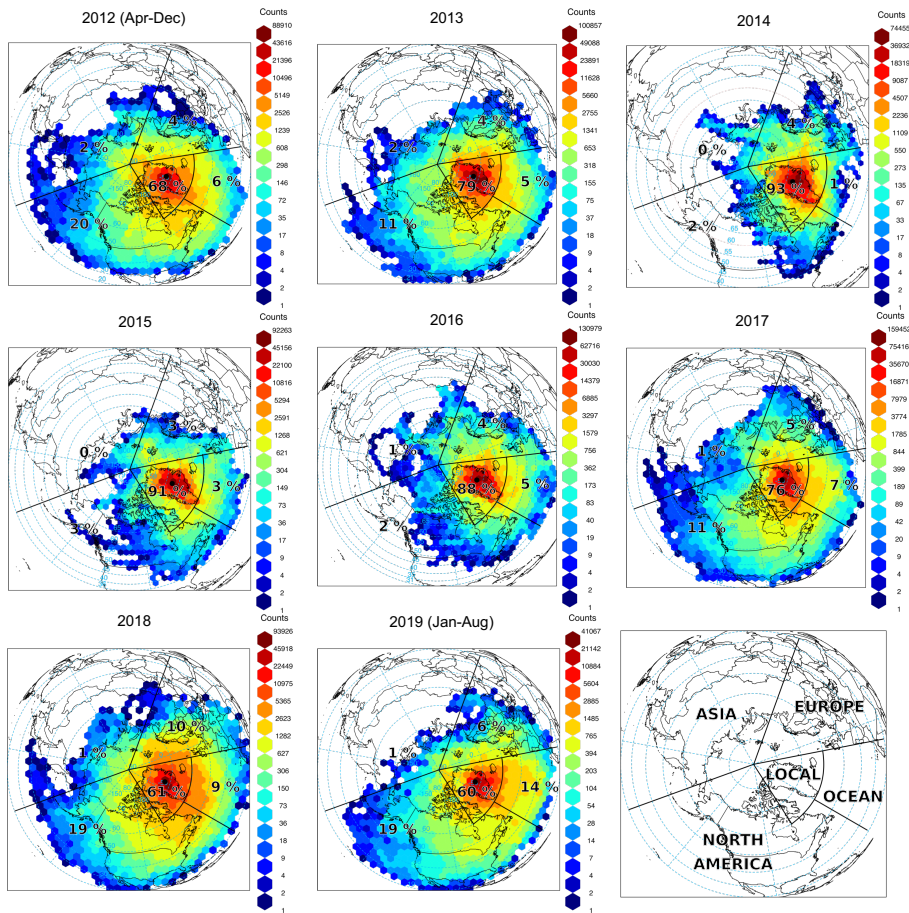


Figure 5: Origin air masses influencing GEOSummit (black dot). Gridded back trajectory frequencies using an orthogonal map projection (centered over the North Pole) with hexagonal binning. The tiles represent the number of incidences and the numbers the relative influence of the various sectors.

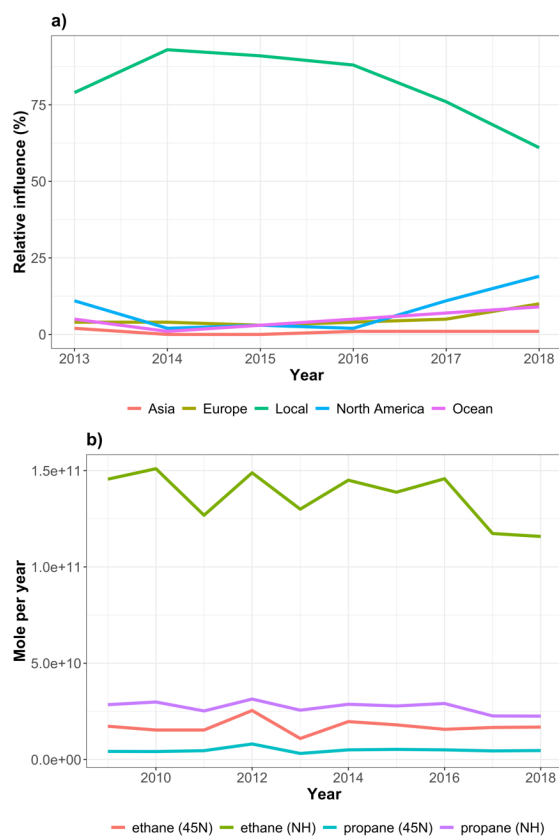


Figure 6: a) Annual relative contribution of different geographical sectors to air masses influencing GEOSummit according to the HYSPLIT back-trajectories analysis. **b)** Annual biomass burning emissions (in mole/year) from all open burning north of 45°N and north of the equator (Northern Hemisphere, NH) according to the Fire INventory from NCAR (FINNv2.2) emission estimates (MODIS only).

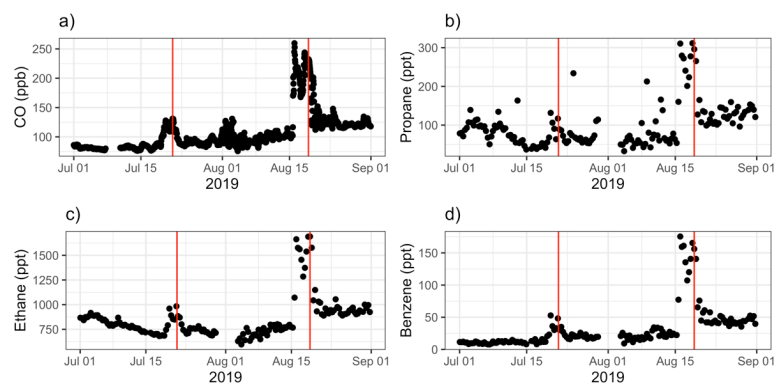


Figure 7: Time-series of **a)** carbon monoxide (CO), **b)** propane, **c)** ethane, and **d)** benzene mixing ratios in ambient air at GEOSummit in July-August 2019. The two vertical red lines show the simultaneous enhancement of mixing ratios in two biomass burning plumes.

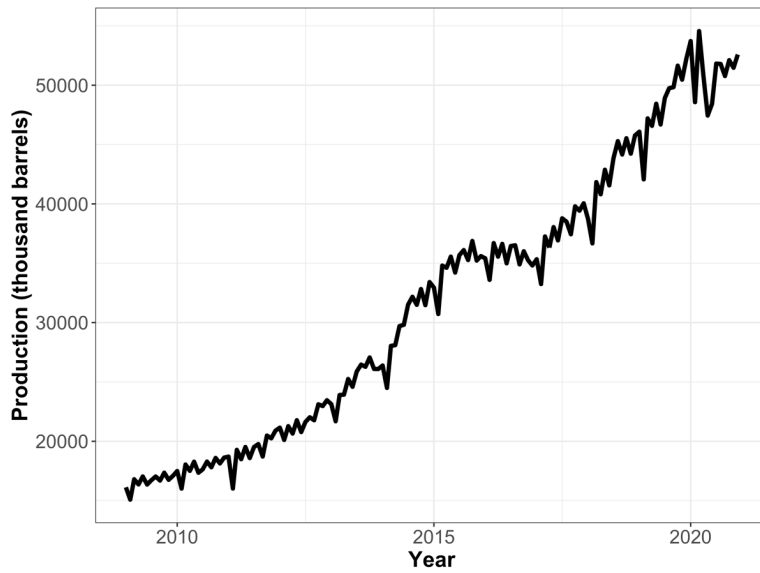


Figure 8: U.S. field production of propane in thousand barrels per month. Data courtesy of the U.S. Energy Information Administration. The production plateaued from June 2014 to December 2016.

